LUND UNIVERSITY

Verification of Dose Calculation Algorithms in Treatment Planning Systems for External Radiation Therapy: A Monte Carlo Approach

Wieslander, Elinore

2006

II

INSTITUTE OF PHYSICS PUBLISHING PHYSICS IN MEDICINE AND BIOLOGY

Phys. Med. Biol. **48** (2003) 3295–3305 PII: S0031-9155(03)60201-0

Dose perturbation in the presence of metallic implants: treatment planning system versus Monte Carlo simulations

Elinore Wieslander and Tommy Knöös

Radiation Physics, Lund University Hospital, SE-221 85 Lund, Sweden

E-mail: elinore.wieslander@skane.se

Received 28 February 2003, in final form 21 July 2003
Published 30 September 2003
Online at stacks.iop.org/PMB/48/3295

Abstract

An increasing number of patients receiving radiation therapy have metallic implants such as hip prostheses. Therefore, beams are normally set up to avoid irradiation through the implant; however, this cannot always be accomplished. In such situations, knowledge of the accuracy of the used treatment planning system (TPS) is required. Two algorithms, the pencil beam (PB) and the collapsed cone (CC), are implemented in the studied TPS. Comparisons are made with Monte Carlo simulations for 6 and 18 MV. The studied materials are steel, CoCrMo, Orthinox®[1], TiAlV and Ti. Monte Carlo simulated depth dose curves and dose profiles are compared to CC and PB calculated data. The CC algorithm shows overall a better agreement with Monte Carlo than the PB algorithm. Thus, it is recommended to use the CC algorithm to get the most accurate dose calculation both for the planning target volume and for tissues adjacent to the implants when beams are set up to pass through implants.

1. Introduction

A small but increasing number of patients receiving radiation therapy today have high-Z implants such as hip prostheses. The size of the dose perturbation due to the high-Z media depends, e.g., on the design and composition of the implant and characteristics of the radiation. Limitations in the treatment planning system (TPS) are the main source of error. For example, the lack of modelling changes in charged particle production and photon scattering due to changes in elemental composition. Therefore, it is recommended to avoid treatments where the fields pass through the high-Z media before they reach the planning target volume (PTV) (Lin *et al* 2002, Roberts 2001, Erlanson *et al* 1991, Biggs and Russell 1988). This is, however, not always possible and therefore knowledge of the accuracy of the TPS is required.

[1] Orthinox®, a stainless steel alloy and registered trademark of Stryker Corporation.

The aim of this work is to use a Monte Carlo (MC) code to benchmark two dose calculation algorithms, the pencil beam (PB) (Ahnesjö *et al* 1992) and the collapsed cone (CC) (Ahnesjö 1989), that are present in the TPS[2], in the presence of metallic inhomogeneities. The geometry studied is a schematic femoral head-like hip prosthesis, but the results can be transformed to other types of implants. The high-*Z* materials studied are Ti, steel, Ti alloy, CoCrMo alloy and Orthinox®, a steel alloy. The majority of the prostheses used in Sweden are made of CoCrMo alloys and are mounted with 'bone cement'. Among the cementless prostheses, Ti alloys dominate.

A Monte Carlo based virtual accelerator has been developed earlier based on the EGS4 user code XYZP (Wieslander and Knöös 2000). The data needed to characterize a treatment unit in the TPS were generated with Monte Carlo simulations, a virtual accelerator. These data were then implemented in the TPS by the vendor, in accordance with the same procedure as used for 'real' accelerators, and made available for treatment planning. No difference was found between the characterization set generated with the EGS4 user code XYZP and the EGSnrc user code dosxyznrc. Therefore, the latter code, due to the improvements in simulations at interfaces, is used in this study. The virtual accelerator and its corresponding unit in the TPS can, e.g., be used for benchmarking dose calculations in geometries and points where it is difficult or impossible to perform measurements. Another advantage is that this approach also avoids deviations in fluctuating accelerator performance compared to the data in the TPS. This virtual accelerator is set up to study the accuracy in a hip-like geometry for 6 and 18 MV x-rays. The pencil beam algorithm of an earlier version of the TPS, in the presence of steel and Ti, has been studied experimentally by Roberts (2001). New features in the present version are the possibility of editing materials and to some extent also densities and an extended list of available materials. These new possibilities aim to improve the accuracy of the TPS.

2. Materials and methods

2.1. The TPS calculation algorithms

The TPS is fluence based and the terma, found after the ray-tracing, is transported using a superposition of either a pencil kernel (PB) or a point kernel (CC) resulting in the absorbed dose distribution. The implementation and accuracy of these models have been reported earlier (Weber and Nilsson 2002, Knöös *et al* 2001). The parameters describing the pencil beam, separated in primary and scatter dose, are pre-calculated and tabulated down to a depth of 50.025 cm. For depths larger than this limit, a simplified dose model with depth dependence added, similar to the analytical expression of the pencil beam kernel, is used (Weber 2003).

During the pencil beam convolution, the primary dose is calculated by using the equivalent-depth model. The phantom scatter dose is calculated for unit density and then corrected with a one-dimensional convolution algorithm considering changes in electron density.

In the collapsed cone model, the deposited terma in each voxel is transported in a fixed number of directions, the so-called cones or pipes. The pipe density is higher in the forward direction, to reflect the pronounced distribution of scattered photons in this direction. When ray-tracing along a pipe through the density matrix, both the electron density and the atomic composition of the tissue are accounted for. To receive the absorbed dose in a voxel, energy deposition from all pipe segments is summed up. These doses are assigned to the centre of the voxels from which the user-specified dose points are 3D interpolated.

[2] Helax-TMS version 6.1 from MDS Nordion Therapy Systems, Uppsala Sweden.

In the TPS the density matrix is mapped from a series of CT images or for phantom construction direct in the system. The Hounsfield numbers (HN) are converted to densities, and a selection of a few standard material/tissue is also determined from the HN. Materials with HN over 2840 are interpreted as iron with a density of 7.87 g cm^{-3}. New features are the possibility of editing materials and to some extent also densities and that the list of available materials has been extended, the following non-tissue high-Z materials are available: aluminium, stainless steel, titanium alloy and lead. Note that if a patient with a Ti alloy implant is CT-scanned and imported into the TPS, the implant is mapped to iron. The implant must be manually edited to the Ti alloy.

The pencil beam algorithm calculates dose to water, which is a consequence of the point-spread functions being generated in water. The collapsed cone and the Monte Carlo, on the other hand, calculate the dose to the medium specified.

2.2. Monte Carlo calculations

The original Monte Carlo based virtual linac implemented in the TPS was performed with EGS4 (Wieslander and Knöös 2000). The module used was the XYZP with PRESTA implemented (Bielajew and Rogers 1987), in which the possibilities of using a photon spectrum and divergent beams were added. Due to the improvements of interface simulations in the EGSnrc code (Verhaegen 2002, Kawrakow 2000a, 2000b, Kawrakow and Rogers 2001), this code was used in this study. The module used was the user code dosxyznrc (Walters and Rogers 2002). All the input data to the TPS were benchmarked with dosxyznrc and no difference was found. The EGS4 code dosxyz, after modifications to separate dose components, has been used to study the modelling of scatter and primary dose in the TPS (Wieslander *et al* 2001).

Depth-dose equivalent spectra extracted from the TPS are used. Throughout the study, the EGSnrc/EGS4 transport parameters AP $= P_{\mathrm{cut}} = 10$ keV and AE $= E_{\mathrm{cut}} = 521$ keV are used, i.e., photons and electrons with energy above 10 keV are modelled explicitly while photons and electrons with energy lower than 10 keV are considered locally absorbed. In EGSnrc the boundary crossing algorithm EXACT with skin-depth 3 mean free path, spin effects turned on and electron-step algorithm PRESTA-II were used. For the materials which did not exist in the NRCC package (Rogers *et al* 2002), PEGS was used with the general description of the density effect (Nelson *et al* 1985).

The simulations are performed with ten batches and the statistical uncertainty, estimated as 1 standard deviation, is kept below 0.8% at all points inside the primary radiation field.

2.3. Dose distribution in a hip prosthesis-like geometry

The virtual accelerator based on Monte Carlo and its corresponding unit in the TPS is used to calculate the dose distribution in a hip prosthesis-like geometry. The geometry used is a $30 \times 30 \times 30$ cm^3 water phantom with a $4 \times 4 \times 4$ cm^3 high-Z cavity, made of various materials, centred at 12 cm depth. In the TPS calculations, Ti alloy and steel are used, and the phantom is constructed directly in the TPS to avoid effects due to beam hardening artefacts and other perturbations that can be introduced in the CT scan. The phantom consists of 60 abutted slices with thickness of 0.5 cm. The MC simulations are performed with cavities made of Ti, steel, CoCrMo, TiAlV and Orthinox®, where CoCrMo, TiAlV and Orthinox® are the three most frequently used alloys for hip prostheses in Sweden. The composition and density of CoCrMo, TiAlV and Orthinox® are in accordance with data from the vendors. Since a Ti alloy and a steel alloy are the only available media in the TPS, Ti and TiAlV are compared to the Ti alloy and CoCrMo, Orthinox® and steel are compared to the steel alloy. For details of the material

Table 1. Main elements and densities of the studied materials.

	Main elements	Mass density (g cm^{-3})
Steel MC/TPS	Fe, Cr, Ni	8.06/7.80
CoCrMo	Co, Cr, Mo	8.22
Orthinox®	Fe, Cr, Ni	7.90
Ti	Ti	4.54
TiAlV MC/Ti alloy TPS	Ti, Al, V	4.34/4.54

used, see table 1. MC simulations with different densities show that the small differences in density between the alloy used in the TPS and the alloy used in the MC simulations result in a TPS calculated dose that is 2.5–3% too high for steel and 1–1.5% too low for the Ti alloy. For CoCrMo and Orthinox® the corresponding figures are 3.5–5% and 0.5–1% too high.

The phantom was irradiated with a 10×10 cm^2 open photon field, set up with a source–phantom distance of 100 cm, and 6 and 18 MV x-rays were applied. The voxel size used in the collapsed cone calculations is $\Delta x = 0.145$, $\Delta y = 0.5$ and $\Delta z = 0.145$ cm, where Δy is the slice thickness. The dose in the MC simulations is scored in a Cartesian voxel system along the z-axis and along the x-axis at 5, 12, 14.5, 16 and 19 cm depths. The voxel sizes were $\Delta x = 0.2$, $\Delta y = 2.0$ and $\Delta z = 0.4$ cm for profiles and $\Delta x = 2.0$, $\Delta y = 2.0$ and $\Delta z = 0.2$ cm for depth doses. For depth doses 100–200 $\times 10^6$ histories have been followed and this number was increased by a factor 10 for profiles in the MC simulations.

3. Results and discussion

Depth-dose and profile data are normalized to 100% at 5 cm depth. Relative errors for depth doses are determined between TPS and MC, as $(D_{\mathrm{TPS}} - D_{\mathrm{MC}})/D_{\mathrm{MC}}$. The characteristics of the central depth-dose curves for CoCrMo and Orthinox® are nearly the same as those for steel, and the characteristics for TiAlV are close to those for Ti. Therefore, central depth-dose curves and profiles at four different depths are presented for steel and titanium cavity for both energies and both algorithms. For the other materials; steel, CoCrMo and Orthinox®, only relative errors are presented.

In figure 1, results for 6 MV and 18 MV x-rays are presented for steel and titanium prostheses. The relative errors for CoCrMo, Orthinox® and TiAlV for both energies are displayed in figure 2 for the pencil beam algorithm and in figure 3 for the collapsed cone algorithm.

For all combinations of energies, algorithms and materials, the agreement is good down to about 1–0.5 cm in front of the high-Z cavity, except in the build-up region at the entrance surface of the phantom. The discrepancy of the dose in the build-up region, calculated with the PB algorithm, is well known. Since the same approach is used in the CC algorithm, improvements are not expected. Inside the high-Z cavity discrepancies between PB and MC are expected since PB calculates dose to water. For steel alloys and CoCrMo, spectrum weighted μ_{en}/ρ ratios (water to high-Z media) are 1.12 and 0.91 for 6 MV and 18 MV, respectively. The corresponding figures for TiAlV and Ti are 1.15 for 6 MV and 0.96 for 18 MV. Since CC calculates the dose to the media, the agreement is much better inside the high-Z media for this algorithm. The remaining discrepancy is due to an underestimation of the phantom scatter component in CC. The PB algorithm does not model interface effects very well due to loss of electron equilibrium. Interface effects upstream are not fully modelled by the collapsed cone algorithm due to the low density of pipes in this direction. The interface effects downstream are modelled much better by the CC but not correctly. Note that both MC and CC data are voxel averages.

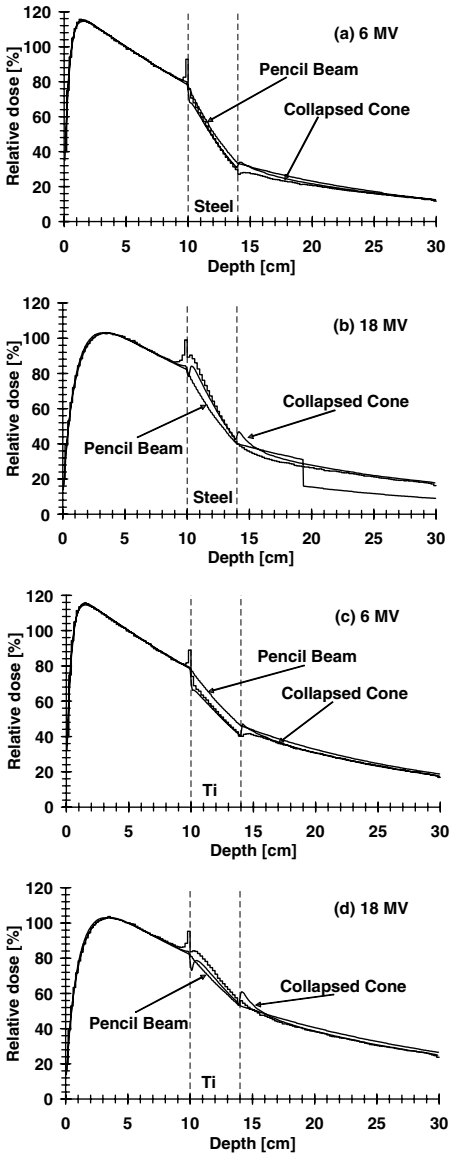

Figure 1. Central depth doses through the steel ((a) and (b)) and titanium ((c) and (d)) cavities for 6 MV and 18 MV. Step-shaped curves represent Monte Carlo simulations and solid lines represent TPS calculations.

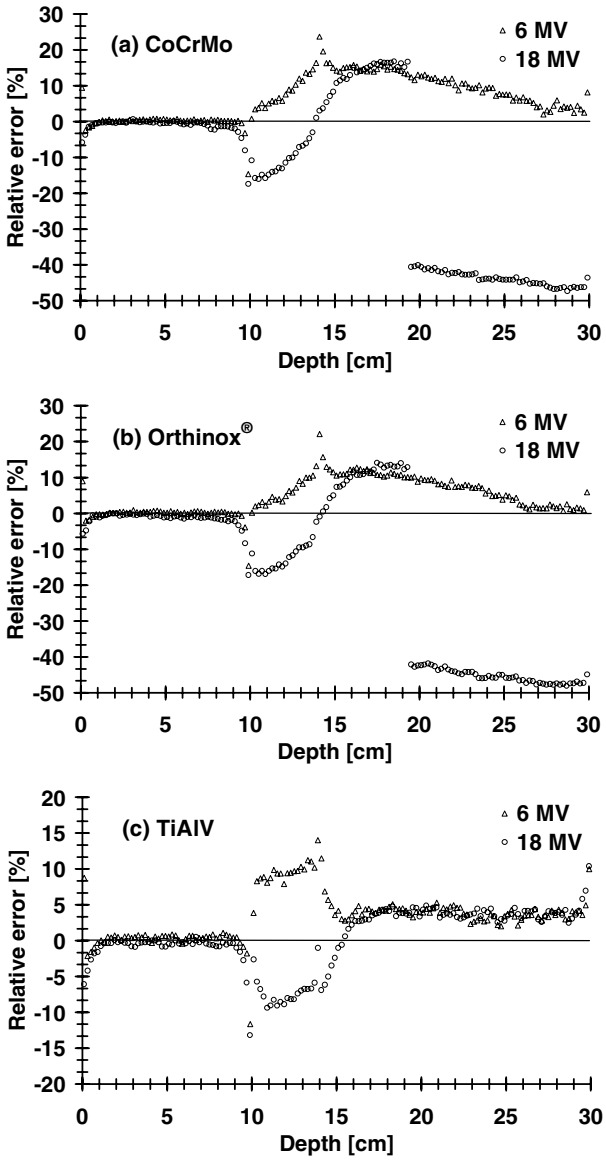

Figure 2. Relative errors, in central depth doses, between the pencil beam algorithm and the Monte Carlo simulations for the CoCrMo (a), Orthinox® (b) and TiAlV (c) cavities for both 6 MV and 18 MV.

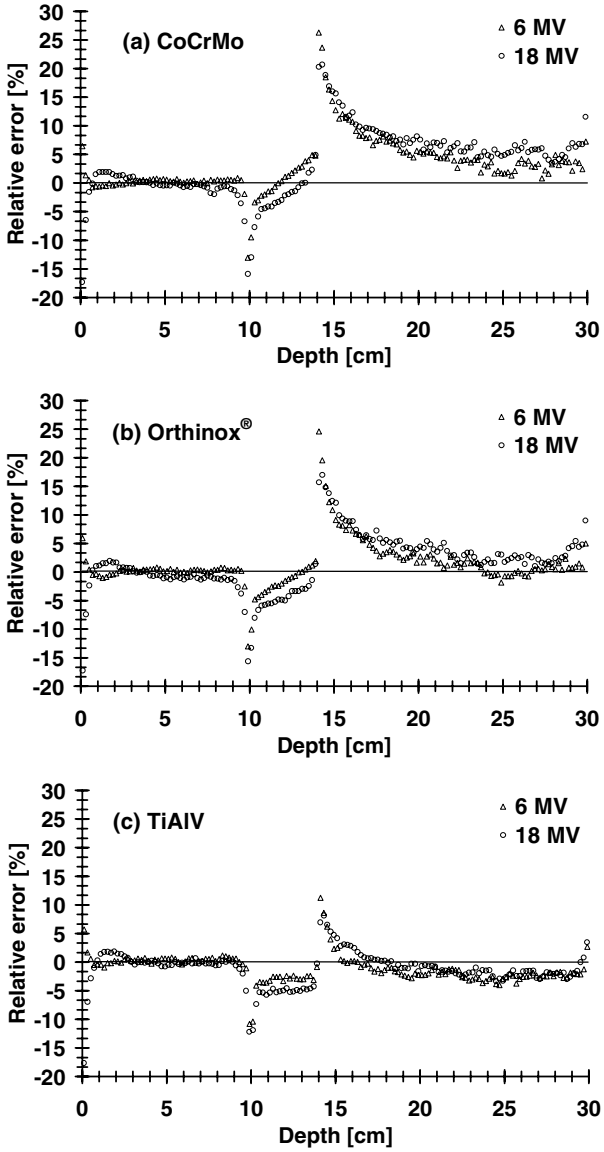

Figure 3. Relative errors, in central depth doses, between collapsed cone algorithm and the Monte Carlo simulations for the CoCrMo (a), Orthinox® (b) and TiAlV (c) cavities for both 6 and 18 MV.

Table 2. Relative errors, in per cent, along the central axis between the TPS and the Monte Carlo simulation, at 6 cm beyond the cavity.

	Relative error, in %, between TPS and MC at 6 cm beyond the cavity			
	6 MV		18 MV	
	PB	CC	PB	CC
Steel	11.7	4.3	−41.5	5.6
CoCrMo	12.6	5.2	−40.6	7.3
Orthinox®	9.5	2.3	−42.4	4.0
Ti	6.4	0.0	6.0	0.8
TiAlV	4.1	−2.2	4.3	−0.8

After the high-*Z* cavity the PB algorithm overestimates the dose for all materials and both energies. The overestimation for TiAlV is due to an inefficient phantom scatter modelling in the PB. The phantom scatter component is also too large for the steel alloys and CoCrMo, but the difference between MC and PB reduces with increasing depth beyond the cavity. The overall deviation beyond the cavity for all materials reveals drawbacks in the correction model for inhomogeneities in the PB algorithm. For an 18 MV field and a cavity of steel, the PB algorithm breaks down at 19 cm depth with large deviations in the dose (radiological depth larger than 50.025 cm). The algorithm that calculates the dose at depths greater than 50.025 cm is either deficient or wrongly implemented. The CC algorithm overestimates the dose for steel, CoCrMo and Orthinox® and underestimates the dose for Ti and TiAlV. The over/underestimation changes only slightly with depth beyond the cavity except in regions of interface effects, since the description of primary and phantom scatter dose is more accurate in the CC algorithm. For the steel alloys and CoCrMo the difference in phantom scatter between CC and MC changes with depth beyond the cavity leading to a small change in relative error with depth compared to TiAlV. The overall deviation beyond the cavity is smaller compared to the PB algorithm, indicating an improved modelling of inhomogeneities in the CC algorithm.

A representative target depth for the lateral fields used for treatments in the pelvic region, e.g., in the four-field box technique, is 20 cm i.e., 6 cm beyond the cavity. The relative errors at 6 cm beyond the cavity are displayed in table 2.

Figure 4 presents profiles for steel and Ti cavity at 5, 12, i.e., trough the cavity, and 19 cm depths for 6 and 18 MV photons for both algorithms. At 5 cm depth the agreement is good between TPS and MC. At 12 cm depth in the H_2O away from the cavity the differences between TPS and MC are small. An example of when the PB algorithm fails is when the electron equilibrium is insufficient combined with changes in density. This is shown in the profiles through the cavity. The energy lost by scattering out from the cavity into the water is not compensated by scatter in to it. Thus the PB will just have a sharp step in the profile reflecting the difference in primary attenuation. Both MC and the CC show the increase of particles/energy scattered out from the cavity. In the interface H_2O–high-*Z* media, there is a local increase in dose due to electrons scattered from the high-*Z* media. In the high-*Z* media there is a local decrease in dose since the electrons that are scattered out from the high-*Z* media are not compensated for. The PB algorithm does not account for these changes in scatter due to lateral inhomogeneities. It always assumes that the lateral scatter medium is water. At larger depths, the agreement between MC and PB is good in areas that are not directly affected by the cavity.

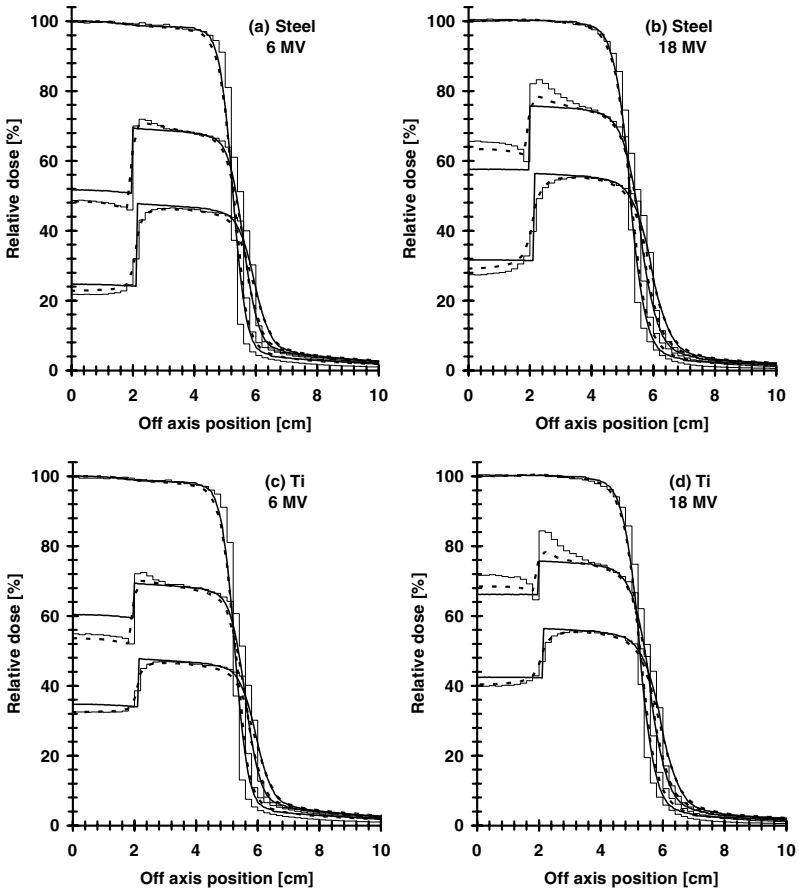

Figure 4. Profiles for the steel ((a) and (b)) and titanium ((c) and (d)) cavity at 5, 12, i.e. trough the cavity, and 19 cm depth for 6 and 18 MV photons for both algorithms. Step-shaped curves represent Monte Carlo simulations, solid lines represent the pencil beam algorithm and dashed lines represent the collapsed cone algorithm.

At 12 cm depth in the H_2O away from the cavity, the differences between CC and MC are small. The interface effects are only partly modelled by the CC algorithm. At larger depths, the agreement between MC and CC is good in all areas.

4. Conclusions

The perturbations due to metallic implants, such as hip prostheses, have been studied by a Monte Carlo technique. The geometry studied has been a schematic femoral head-like hip

prosthesis, but the results can be transformed to other types of implants. The limitations of a commercial TPS have been shown. For dose determination by the TPS, the composition and design of the implant must be known. Beam hardening artefacts in the CT data make it difficult to outline the contour and interior of the implant. Thus the voxels occupied by the implant must be edited manually to obtain the correct material. The material of the implant must also be present among the available materials in the TPS. The density of the high-Z materials in the TPS cannot be changed and therefore discrepancies in dose will occur due to differences in density.

This study shows that it is possible to determine the dose quite accurately away from cavities of different steel alloys, Ti, TiAlV and CoCrMo, using the CC algorithm. At 6 cm beyond the cavity, the calculated dose is within −2.2–5.2% for 6 MV and −0.8–7.3% for 18 MV compared to MC. The effects due to loss of electron equilibrium are improved in the CC algorithm compared to the PB algorithm, especially in the high-Z region. For Ti and TiAlV the PB algorithm calculates the dose within 4–6% beyond the cavity for both energies, but it does not handle effects due to loss of electron equilibrium. For the two steel cavities and the CoCrMo cavity, the dose is calculated with the PB algorithm within 4–15% for 6 MV depending on the depth beyond the cavity. The use of a steel cavity and an 18 MV field in the TPS together with the PB algorithm leads to large discrepancies. This is due to the simplified dose engine at depths larger than 50.025 cm. Note that the PB algorithm calculates dose to water and not dose to the specified media as both the CC algorithm and MC do. The difference in dose between PB and MC in the high-Z cavity is therefore due to both differences in elemental composition between water and the high-Z media and drawbacks of the PB algorithm.

With knowledge of the behaviour of the TPS in the presence of metallic inhomogeneities, the benefits and drawbacks of allowing the fields to pass through the high-Z cavity before the PTV can be evaluated. The use of the CC algorithm is recommended for treatment requiring fields passing through the implant before they reach the PTV. Thus, problems with the PB at large depth and especially its deficient modelling adjacent to the implant are avoided.

Acknowledgments

The support and funding by the Lund University Hospital Funds and the John and Augusta Persson's Foundation for Scientific Medical Research are greatly appreciated. The referees who improved the paper with their comments and recommendations are also acknowledged.

References

Ahnesjö A 1989 Collapsed cone convolution of radiant energy for photon dose calculation in heterogeneous media *Med. Phys.* **16** 577–92

Ahnesjö A, Saxner M and Trepp A 1992 A pencil beam model for photon dose calculation *Med. Phys.* **19** 263–73

Bielajew A F and Rogers D W O 1987 PRESTA: the parameter reduced electron-step algorithm for electron Monte Carlo transport *Nucl. Instrum. Methods. Phys. Res.* B **18** 165–81

Biggs P J and Russell M D 1988 Effect of femoral head prosthesis on megavoltage beam radiotherapy *Int. J. Radiat. Oncol. Biol. Phys.* **14** 581–6

Erlanson M, Franzén L, Henriksson R, Littbrand B and Löfroth P-O 1991 Planning of radiotherapy for patients with hip prosthesis *Int. J. Radiat. Oncol. Biol. Phys.* **20** 1093–8

Kawrakow I 2000a Accurate condensed history Monte Carlo simulation of electron transport: I. EGSnrc, the new EGS4 version *Med. Phys.* **27** 485–98

Kawrakow I 2000b Accurate condensed history Monte Carlo simulation of electron transport: II. Application to ion chamber response simulations *Med. Phys.* **27** 499–513

Kawrakow I and Rogers D W O 2001 The EGSnrc system, a status report Advanced Monte Carlo for radiation physics, particle transport simulation and applications *Proc. Monte Carlo 2000 Conf. (Lisbon, 23–26 Oct. 2000)* ed A Kling, F Barão, M Nakagawa, L Távora and P Vaz (Berlin: Springer) pp 135–40

Knöös T, Karolak L and Nilsson P 2001 Quantification of dosimetry changes in a TPS after implementation of a new dose calculation algorithm: pencil beam vs. collapsed cone *Radiother. Oncol.* **61** S22

Lin S-Y, Chu T-C, Lin J-P and Liu M-T 2002 The effect of a metal hip prosthesis on the radiation dose in therapeutic photon beam irradiations *Appl. Radiat. Isot.* **57** 17–23

Nelson W R, Hirayama H and Rogers D W O 1985 The EGS4 code system Stanford Linear Accelerator Center *SLAC-Report*-265

Roberts R 2001 How accurate is a CT-based dose calculation on a pencil beam TPS for a patient with a metallic prosthesis? *Phys. Med. Biol.* **46** N227–N234

Rogers D W O, Ma C M, Walters B, Ding G X, Sheikh-Bagheri D and Zhang G 2002 BEAMnrc users manual *National Research Council of Canada Report* PIRS-0509(A)revG

Verhaegen F 2002 Evaluation of the EGSnrc Monte Carlo code for interface dosimetry near high-Z media exposed to kilovolt and ^{60}Co photons *Phys. Med. Biol.* **47** 1691–705

Walters B R B and Rogers D W O 2002 DOSXYZnrc users manual *National Research Council of Canada Report PIRS-709*

Weber L and Nilsson P 2002 Verification of dose calculations with a clinical treatment planning system based on a point kernel dose engine *Appl. Clin. Med. Phys.* **3** 73–87

Weber L 2003 Personal communication

Wieslander E and Knöös T 2000 A virtual linear accelerator for verification of treatment planning systems *Phys. Med. Biol.* **45** 2887–96

Wieslander E, Sheikh-Bagheri D, Weber L, Ahnesjö A and Knöös T 2001 Monte Carlo verification of a multi-source model used in a treatment planning system *Radiother. Oncol.* **61** S101